Electron Thermal Transport in NSTX and Tore Supra

W. Horton, H. V. Wong, P.J. Morrison, A. Wurm, J.C. Perez, J.H. Kim
Institute for Fusion Studies, The University of Texas at Austin, Austin, Texas, 78712, USA

G. T. Hoang
Association Euratom-CEA, CEA/DSM/DRFC,
CEA Cadarache, 13108 Saint-Paul-Lez Durance, France

B. P. LeBlanc
Plasma Physics Laboratory, Princeton University, Princeton, NJ 08543
(Dated: October 15, 2004)

A transport analysis of Tore Supra (TS) and NSTX discharges with centrally deposited fast wave electron heating is performed, and electron thermal fluxes are derived from power balance. Measurements of the electron temperature and density profiles, combined with ray tracing computation of the power deposition, allow detailed interpretation of the thermal flux versus temperature gradient. Evidence supporting the occurrence of electron temperature gradient (ETG) turbulent transport in the two confinement devices is found. Evidence for this mechanism includes: (1) a consistent scaling in density and temperature in both the profiles and radial heat flux, (2) a clear analytical and fundamental thermodynamic origin for the critical temperature gradient and its dependence on magnetic shear, (3) insensitivity of the turbulence to the mixture of trapped and passing electrons, (4) self-consistent turbulent generation of a magnetic flutter component from the parallel electron currents, and (5) good agreement between the thermal flux formulas used in radial transport codes with auxiliary heating and the profiles measured both in radius and time. Finally, internal transport barriers created in certain TS and NSTX discharges are argued to be a universal feature of transport equations in the presence of a (partially broken) invariant torus that is generic to nonmonotonic rotational transforms in dynamical systems. Weakly reversed magnetic shear discharges in NSTX show improved confinement in L-mode discharges.

1. Electron Transport in Tokamaks

Turbulent transport of electron thermal energy appears to be ubiquitous in tokamaks. This suggests that it may arise from small space and time scales associated with electron temperature gradient-driven drift wave turbulence (ETG). Simulations show that while the source of the turbulence is on the scale of the electron gyroradius ρ_e, the nonlinear saturated states have large-scale structures on the scale of the collisionless skin depth. Various numerical simulations with two-component fluids, gyrofluids, and gyrokinetics show levels of electron diffusivity comparable to that of the ion thermal transport from ITG-driven turbulence. These results support the general conclusion of Kadomtsev [1] that there is an intrinsic level of anomalous electron turbulent transport in toroidal confinement devices. For higher values of $\beta_e = 2\mu_0 p_e/B^2$ and not too low a plasma density, the characteristic scale length is the collisionless skin depth $\delta_s = c/\omega_{pe}$, owing to the intrinsic inductive electric field from the magnetic fluctuations. New derivations of the dynamical equations using the linearized drift kinetic equation to close the moment equations have been obtained which avoid the specification of the adiabatic gas constant in the electron pressure equation.

The time scale is that of the microscale electron dynamics $\tau_e = R/v_e$. Particular theoretical formulas developed for the electron thermal fluxes with critical gradients have successfully interpreted transport in Tore Supra with Fast Wave Electron Heating, where thermal fluxes and gradients vary over an order of magnitude in response to RF power increasing from 0.7 MW to 7.5 MW [2–4]. These are high electron beta, helium discharges with 0.65 MA/2.2 T in a classic tokamak geometry with R/a = 2.2 m/0.7 m.

An example for Tore Supra is shown in Fig. 1a using the integrated CRONOS transport code [5] with the ETG transport model for a stair-stepped Fast Wave heating profile of 3 MW and 6 MW. This TS discharge #18368 has $I_p = 0.65$ MA, $B = 2.2$ T, $n_e(0) = 4 \times 10^{19}$ m^{-3} and $T_e(0) = 4$ keV with the fast wave power rising from 3 MW to 6 MW. The time evolution of the electron temperature $T_e(r,t)$ at various radii, the electron energy content $W_e = \frac{3}{2}\int p_e d^3x$, the loop voltage $V_l(t)$, and the Faraday rotation angles are shown in Fig. 1.

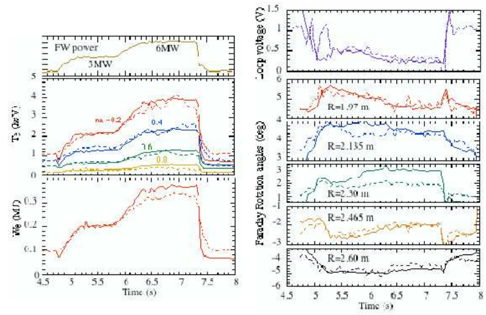

FIG. 1: Tore Supra FWEH discharge #18368 data (dashed curve) compared with the ETG model (solid curve)

The electron transport formulas derived in Horton et al. [4] for Tore Supra and applied to NSTX for similar plasma conditions, but strongly different geometry [6], give similarly good results. For the low-aspect ratio $R/a = 0.85\ m/0.68\ m$ of NSTX, the fraction of trapped electrons reaches 90% in the outer regions so that the trapped electron mode (TEM) instability is potentially a stronger transport mechanism than the ETG mode. Thus, we analyze High Harmonic Fast Wave heated deuterium and helium discharges with the ETG and TEM thermal flux formulas.

As in Tore Supra, the magnetic shear profile is a critical element in the transport behavior while the toroidal plasma rotation is negligible in the RF driven plasmas. The HHFW discharges with RF power up to 2.5 MW delivered in the core electrons are shown in Fig. 2 (for the discharge #106194). The data is shown against the square root of the normalized poloidal field, scaled to NSTX's nominal minor radius of 68 cm. This procedure although not entirely true to real space, reproduces the relevant salient profile features. Electron power balance analysis gives the thermal flux in Fig. 2c and the thermal diffusivity increases with radius as shown in Fig. 2d.

In TS [7] and NSTX [6], reversed magnetic shear profiles appear to partially block the transport of electron guiding centers due to the formation of a shearless invariant torus in the corresponding drift wave transport modeling. An understanding of the persistence of such transport barriers in the weak, and especially reversed, shear case can be gained by considering low order resonances in the drift wave model [8]. (See [9], where the basic ideas are investigated in the closely analogous context of Rossby waves in a shear flow.)

The destruction of a toroidal barrier between two resonances occurs when perturbations increase to the point where resonances overlap. The lowest order resonances are usually the largest, and hence their effect is dominant on transport. The farther the barrier is away from low order resonances, the more robust it is. This idea can be quantified in terms of number theoretical properties of the winding number (q-profile) of the barrier: the more irrational the number, the harder it is to approximate by rational numbers because it lies further away from low order resonances[10]. The effect of an almost flat q-profile is to reduce the density of resonances, i.e., the distance between the main resonances is large, and therefore small perturbations will not result in overlap.

In the reversed shear case, the barrier at $q_{\min}$, the shearless invariant torus, lies in a region where the density of resonances is very low. In contrast to monotonic q-profiles, resonances exist in pairs in reversed shear regions, on opposite sides of $q_{\min}$. In addition to resonance overlap on each side of the barrier, the new phenomenon of separatrix reconnection between resonances pairs occurs, which for not too large perturbations results in in creation of a *new* transport bar-

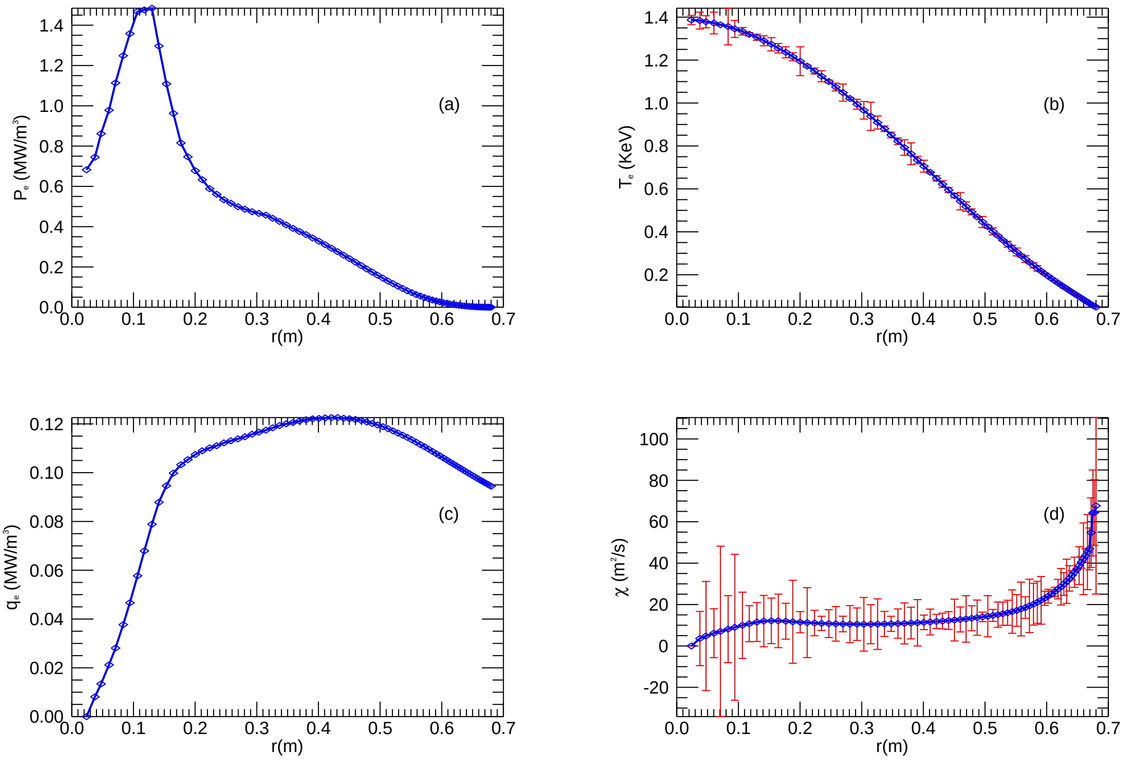

FIG. 2: NSTX profiles for discharge #106194

rier outside of the resonances after the destruction of the central barrier. The detailed break-up of shearless invariant curves depends on the stability of resonances of all orders, whose analysis requires renormalization group techniques [11].

For optimized deuterium HHFW discharges (Fig. 3), a regime of weakly reversed magnetic shear is achieved where χ_e drops to 2-3 m^2/s (the q profile has been obtained from TRANSP analysis [12]). This mode of operation is conducive to centrally peaked T_e profile nearing 4 keV, with an inflection point (foot) around r/a =0.4 in Fig 3b. Here the reversed magnetic shear reduces the ETG growth rate and changes the topology of the electron guiding-center phase space [9]. Surface of section plots of the electron guiding centers show the formation of shearless invariant curves in the associated poloidal surface of section [11]. Correlated with this improved electron confinement is the accumulation of impurity ions and a rise in the axially-peaked $Z_{\rm eff}$ from 2.8 to 3.8. Figure 4 supports the hypothesis that ETG turbulence can explain the electron power balance channel in the HHFW discharges in NSTX.

The combination of the low aspect ratio NSTX and the high aspect ratio Tore Supra classic circular cross-section tokamak, both with high-power, fast-wave electron heating, make an ideal combination for electron transport research. The fact that the ETG model is able to explain the electron power balance heat flux in both of these machines is strong evidence for the validity of the model.

The NSTX and TS tokamaks provide data with a wide range of values for six key dimensionless parameters: temperature ratio T_i/T_e, aspect ratio R/a, trapped electron fraction $(B_{\rm max}/B_{\rm min})$ on a magnetic surface, electron collisionality ν_{*e}, the gradient parameters η_i and η_e, plasma pressure β_e, and magnetic safety factor q and shear $s = rq'/q$. Both have high-power auxiliary FW heated plasmas with 90% of the RF power (3 MW into 4-5m ^{3} for NSTX and 7 MW in 6 m^3 for TS) giving a clear electron power balance channel for study of the anomalous electron thermal flux q_e(MW/m^2). Both tokamaks show a rapid increase of T_{eo} and ∇T_e up to 12 keV/m for this similar level of core RF power per electron. NSTX discharge #106194

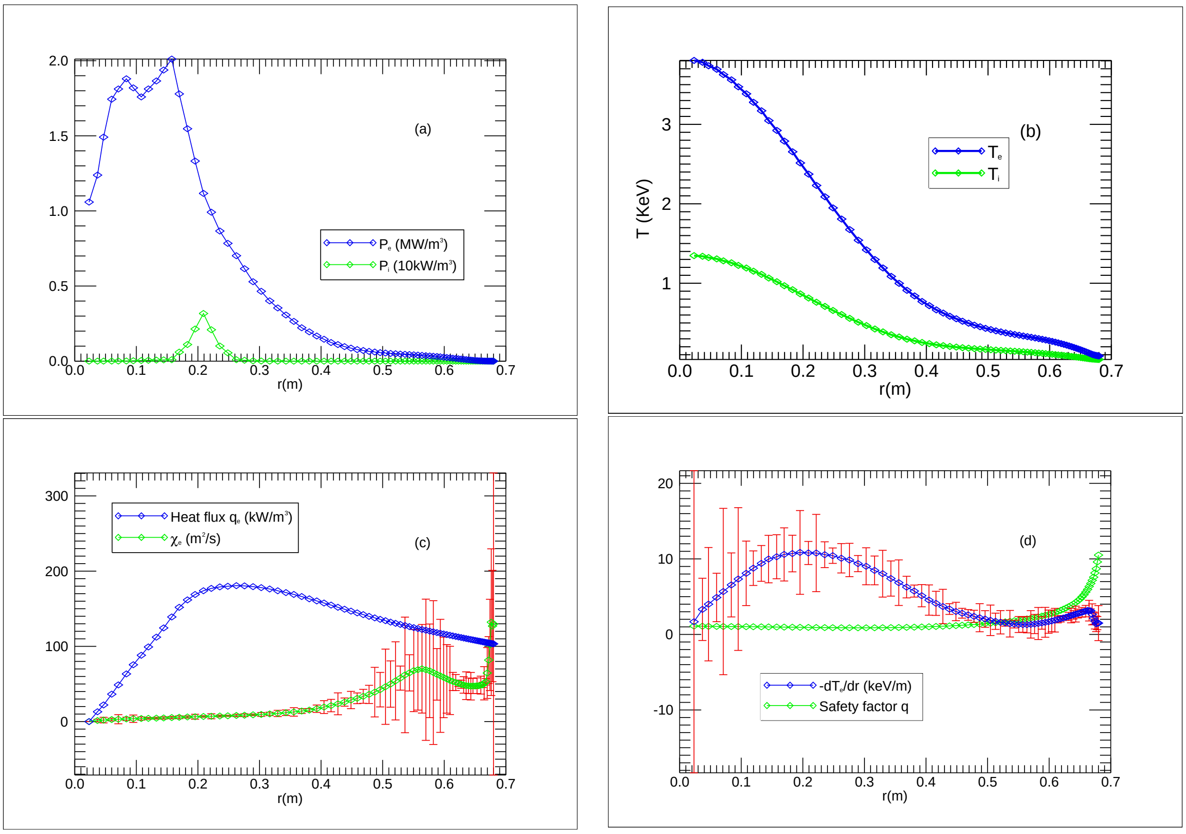

FIG. 3: NSTX profiles for reversed magnetic shear discharge #105830

with He working gas, with an L-mode edge and peaked density profile has an H-mode-like global confinement time of 30 ms with $H_{97\mathrm{L}} \sim 2$. Tore Supra also has peaked density profiles with $H_{97\mathrm{L}} \sim 1.7$ in L-mode He plasmas. Figure 3 shows that an optimized 2.15 MW NSTX discharge #105830 with reversed q-profile produces an internal electron transport barrier at $R_{\mathrm{ITB}}/R_0 = 1.4\mathrm{m}/1.0\mathrm{m}$, lasting for about $4\tau_E$ until the peaked ($T_{e0} = 4$ keV) electron profile collapses from a magnetic reconnection event.

Stability calculations suggest that the trapped electron mode, where 50-90% of the electrons are trapped in NSTX beyond $R/R_0 > 1.3$, produces the large anomalous χ_e. In the core region the electron transport is lower, being driven by the electromagnetic ETG transport in the high $\beta_e \sim 10\%$ collisionless plasma. In the core region the magnetic geometry and the plasma conditions are similar to TS where extensive parametric studies over a 40-discharge database confirm the presence of a heat flux $q_e = -n_e\chi_e[\nabla T_e - (\nabla T_e)_c]$ with a collisionless skin depth scaling of $\chi_e^{\mathrm{ETG}} \sim T_e^{1/2}/n_e$ and the linear theory values of the critical gradient $(\nabla T_e)_c$ ([2–4]).

The source of the electron temperature gradient (ETG) turbulence is the high power density P_{rf} deposited in the core of the NSTX plasma by high harmonic fast wave heating. We focus on the discharge #106194 with $P_{\mathrm{rf}} = \int d^3x p_{\mathrm{rf}} = V\bar{P}_{\mathrm{rf}} = 3.3$ MW into the core plasma volume $V = 3 - 4$ m^3. The total plasma volume is $V_T = 11$ m^3.

The local electron power balance equation is

$$\frac{\partial}{\partial t}\left(\frac{3}{2}nT_e\right) + \nabla\cdot\left(\frac{3}{2}nT_e\mathbf{v} + \mathbf{q}\right) + nT_e\nabla\cdot\mathbf{v} = p_{\mathrm{rf}} - p_{\mathrm{edge}} \qquad (1)$$

where the RF power per unit volume is $p_{\mathrm{rf}}(r) \approx p_{\mathrm{rf}}^{(0)}e^{-r/L_{\mathrm{rf}}}$ and p_{edge} arises up in crossing the last closed flux surface. Taking the particle sources as zero in the discharge so that

$$\frac{\partial n}{\partial t} + \nabla\cdot(n\mathbf{v}) = 0; \qquad m_e n_e \frac{d}{dt}v_{\|e} = -enE_\| - \nabla_\| p_e + \frac{m_e\nu_e}{e}j_\|, \qquad (2)$$

we obtain three partial differential equations governing the electron turbulence. We separate $T_e = T_{e0} + \delta T_e$ and introduce the dimensionless variables $\delta T_e/T_{e0} = (\rho_e/R)\delta\hat{T}_e$, $e\varphi/T_e = (\rho_e/R)\hat{\varphi}$, $A_\parallel/B_z\rho_e = (\rho_e/R)\hat{A}$, where $\rho_e = m_e v_e/eB$ and $v_e = \sqrt{T_e/m_e}$, and obtain

$$\mathbf{v}_E = \frac{1}{B}\mathbf{e}_z \times \nabla\varphi = \frac{\rho_e v_e}{R}\mathbf{e}_z \times \hat{\nabla}\varphi; \quad \mathbf{q}_e = \left\langle \frac{3}{2} n T_e \mathbf{v} \right\rangle = -\frac{3}{2} n_e v_e T_e R \left(\frac{\rho_e}{R}\right)^2 \left\langle \delta\hat{T}_e \frac{\partial\hat{\varphi}}{\partial y} \right\rangle. \quad (3)$$

The isotropic ETG model we consider here is given by the following set of three coupled PDEs

$$\begin{aligned}
\left(1-\nabla_\perp^2\right)\frac{\partial\hat{\varphi}}{\partial t} &= \left[1-4\epsilon_n+(1+\eta_e)\nabla_\perp^2\right]\frac{\partial\hat{\varphi}}{\partial y}+2\epsilon_n\frac{\partial\delta\hat{T}_e}{\partial y}+\left[\hat{\varphi},\nabla^2\hat{\varphi}\right]+\partial_\parallel^{nl}\nabla_\perp^2\hat{A}-\mu\nabla^4\hat{\varphi}\\
\left(\nabla^2-\frac{\beta}{2}\right)\frac{\partial\hat{A}}{\partial t} &= \frac{\beta}{2}\left(1+\eta_e\right)\frac{\partial\hat{A}}{\partial y}+2\partial_\parallel^{nl}\hat{\varphi}-\partial_\parallel^{nl}\delta\hat{T}_e-\left[\hat{\varphi},\nabla^2\hat{A}\right]-\frac{\eta}{\mu_0}\nabla^2\hat{A}\\
\frac{\partial\delta\hat{T}_e}{\partial t} &= S_{\rm rf}(r)-s_{\rm edge}(r)-\left[\eta_e-4\epsilon_n(\Gamma-1)\right]\frac{\partial\hat{\varphi}}{\partial y}-2\epsilon_n(2\Gamma-1)\frac{\partial\delta\hat{T}_e}{\partial y}\\
&\quad -(\Gamma-1)\partial_\parallel^{nl}\nabla^2\hat{A}-\left[\hat{\varphi},\delta\hat{T}_e\right]+\chi_\perp\nabla_\perp^2\delta\hat{T}_e+\chi_\parallel\left(\partial_\parallel^{nl}\right)^2\delta\hat{T}_e \qquad (4)
\end{aligned}$$

where $\beta = 2\mu_0 p_e/B^2$, $\eta_e = d\ln T_e/d\ln n_e = L_{ne}/L_{T_e}$ and $\epsilon_n = L_n/R$. The space-time scales used in eqns. (4) are ρ_e and R/v_e. The dimensionless RF source function is $S_{\rm rf} = RP_{\rm rf}/\frac{3}{2}\frac{\rho_e}{R}nT_e v_e \sim O(1)$ and the sink function is such that $\int d^3x\,(S_{\rm rf} - s_{\rm edge}) = 0$ so that a steady state is reached. For NSTX we have $nT_e \sim 10^4$ Pa and $v_e\rho_e = T_e/B \sim 10^3$ m^2/s. Thus $\frac{3}{2}nT_e v_e \rho_e/R^2 \sim 10^7$ W/m^3 and $S_{\rm rf} \sim 0.1$.

A new system of equations with anisotropic pressure is being used to improve the original FLR two-component fluid equations, with the divergence of the momentum stress tensor calculated with the gyrokinetic equation for the electrons.

We integrate eqns. (4) for $\beta = 0.02$, $\epsilon_n = 0.1$, $\eta_e = 2$ using a pseudospectral method on a rectangular grid of 512×2048. Figure 4 shows the dimensionless temperature profiles at early ($tv_e/R = 60$) and late ($tv_e/R = 80$) times with well defined vortices. At later times the entire region between the source and sink (shown clearly in the earliest time frame) is filled with plasma turbulence containing many space scales. The simulation keeps the $k_x = 0$ and $k_y = 0$ modes corresponding to streamers and zonal flows.

2. Eigenmode Spectrum of Fluctuations

The linearized dimensionless equation is $M_k \frac{dy_k}{dt} = L_k y_k$ where the matrix $M_k = \mathrm{diag}\left(1 + k_\perp^2, \beta/2 + k_\perp^2, 1\right)$ and $y_k^T = (\varphi_k\ A_k\ P_k)$. The components of the matrix $L_k = L_k + L^{\rm diss}$ are

$$\begin{array}{lll}
L_{11} = ik_y\left[1-2\epsilon_n-(1+\eta_e)\,k_\perp^2\right] & L_{12} = -ik_z k_\perp^2 & L_{13} = ik_y\epsilon_n\\
L_{21} = -ik_z & L_{22} = -i\frac{k_y\beta}{2}\left(1+\eta_e\right) & L_{23} = ik_z\\
L_{31} = -ik_y\left[\eta_e-2\epsilon_n\left(1+\tau\right)\Gamma\right] & L_{32} = ik_z\Gamma k_\perp^2 & L_{33} = -2ik_y\epsilon_n\left(\Gamma-1\right)
\end{array} \qquad (5)$$

with $L_k^{\rm diss} = -k_\perp^2\,\mathrm{diag}\left(k_\perp^2/R, 1/R_m, \chi\right)$, where the superscript represents the transpose operation.

The ratio of specific heat, Γ is equal to $[1, 5/3, 2]$, corresponding to isothermal, 3D adiabatic, and 2D adiabatic electron fluid. Gyrokinetic equations eliminate Γ. The eigenvalue problem is solved numerically for $k = (k_y, k_z)$ at each radius r, e.g., for NSTX $r = 0.6$ m where the parameter values are $\epsilon_n = 0.18$ $\eta = 1.70$, $\beta = 0.0052$, $\Gamma = 5/3$, $\mu = 1 \times 10^{-4}$, $\chi = 1 \times 10^{-4}$, $\eta/\mu_0 = 1 \times 10^{-4}$. The results show a wide range of ETG turbulence in both tokamaks.

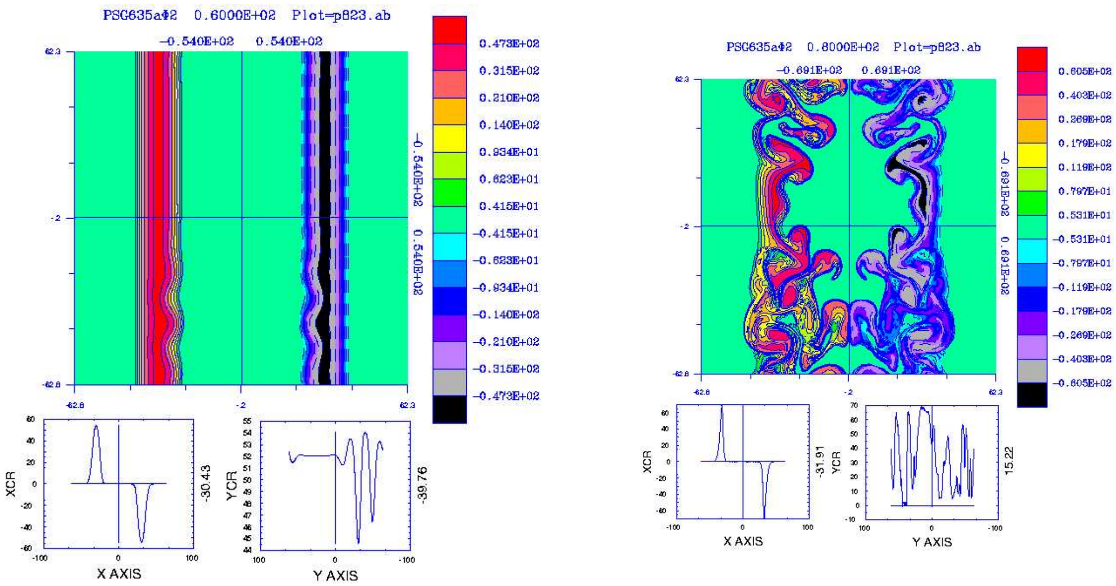

FIG. 4: Simulated temperature profiles for early and late times

3. Comparison with Electrostatic Models and the Trapped Electron Mode

In the limit in which the magnetic vector potential is dropped, the eigenvalue problem reduces to two equations: the vorticity (or charge conservation) equation and the electron thermal balance equation. The dispersion relation is a quadratic equation describing the local toroidal ballooning electron interchange mode. In this case the maximum growth rate occurs for $k_y^{\max} = [(1-2\epsilon_n)/(1+\eta_e)]^{1/2}$ and scales as $\gamma_{max} = (v_e/R)(\eta_e - \eta_c)^{1/2}$ where η_c is the critical gradient. The quasi-two-dimensional $\varphi_k - T_k$ turbulence grows up and drives the electromagnetic turbulence. Thus, the electron temperature gradient is a heat engine, working on plasma, whose output drives thermal transport and the creation of small scale turbulent magnetic fields [13]. Magnetic turbulence with the appropriate character measured in TS [14–16] was originally thought to be the source of the large χ_e transport.

The short wavelength turbulence couples to the long wavelength turbulence that is also driven independently by the ballooning mode in the bounce averaged grad-B/curvature guiding center drifts. Here, however, only the trapped electrons contribute, so the mode is named the Trapped Electron Mode or TEM. While the turbulence on this scale length adds to the overall electron heat flux, it is not as fundamental or as universal in nature as that on the electron time-space scale. The TEM mode, known from the early 1970s, has several well known difficulties in explaining electron transport: (1) the radial profiles of χ_e and the associated heat flux are strongly decreasing functions of minor radius; (2) there is no clear electron temperature gradient threshold in the model, but instead the model gives a critical gradient for the ion temperature gradient and can readily exist with zero electron temperature gradient; (3) the turbulence level is sensitive to the fraction of trapped electrons and weak in machines and radii where the trapped fraction is low; (4) there is no intrinsic magnetic flutter with the mode and in fact increasing the plasma pressure measured by the MHD $\alpha = -q^2 R\mu_0 dp/B_T^2 dr$ stabilizes the mode through a subtle effect involving the geodesic component of the magnetic curvature vector and the radial wavenumber of the eigenmodes; (5) the use of the χ_e^{TEM} formulas in predictive transport code simulations produces profiles in poor agreement with the experimental data and used in globally integrated modeling produces a global energy confinement law that disagrees with the global ITER database confinement laws. By having ETG as the primary source of the electron transport and the TEM as a secondary or supplemental mechanism the interpretative codes give the observed properties of the electron transport.

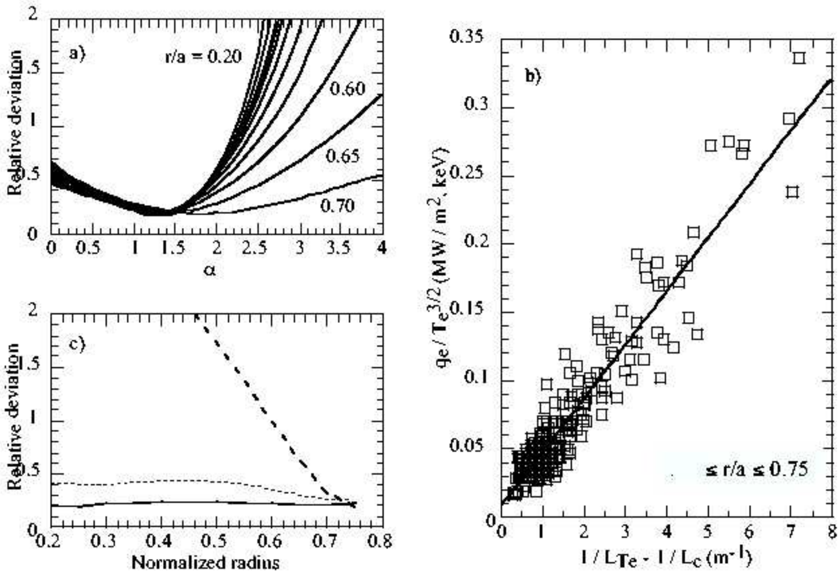

FIG. 5: The scaling exponents on temperature and density for the model heat flux versus the experimental heat flux. (a) gives the optimal exponent $\alpha = 1.5$ for the T_e dependence, (b) shows the well defined critical gradient of the thermal flux scaled by $T_e^{3/2}$ versus the temperature gradient for a large number of shots in Tore Supra and (c) shows the relative deviation of the heat flux normalized to $T_e^{3/2}$ (solid) compared with $n_e T_e^{5/2}$ (dashed) and $n_e T_e^{3/2}$ (dotted).

Figure 5 shows the scaling $q \sim n^\beta T^\alpha$ of the transport that is consistent with an inductive parallel electric field $\partial A_\|$, substracting from the parallel electrostatic field, giving rise to the the two electromagnetic electron-MHD branches. Figure 5a shows the relative deviation of the model from the data for the exponent α in the heat flux, and Fig. 5b shows the scaling of the dimensionless heat flux for the optimal value of $\alpha = 3/2$ with the deviation of the temperature gradient $1/L_{Te} - 1/L_{Te,crit}$ for a wide range of data points over many discharges and positions within a single discharge. Figure 5c shows the relative deviation of the normalized heat flux for the electromagnetic scaling of $q_e \sim T_e^{3/2}$ (solid line with lowest deviation) compared with two electrostatic scalings $q_e/(nT_e^{3/2})$ (dotted line) and $q_e/(nT_e^{5/2})$ (dashed line) for the ITG-TEM mode.

4. Conclusions and Discussion

Transport analyses of Tore Supra and NSTX discharges with centrally deposited fast wave electron heating leads to the conclusion that the the electron temperature gradient instability provides a reliable baseline model for the electron transport. Measurements of the electron temperature and density profiles, combined with results from fast wave RF computations for the power deposition, allow detailed interpretation of the electron thermal flux versus temperature gradient. Evidence supporting the electron temperature gradient (ETG) turbulent transport in these two confinement devices includes: (1) a consistent scaling in density and temperature both in the profiles and parametric variations, (2) a clear analytical and fundamental thermodynamic origin for the critical temperature gradient and its dependence on magnetic shear [3], (3) the turbulence is not particularly sensitive to the mixture of trapped and passing electrons [4], (4) the turbulence generates self-consistently a magnetic flutter component from the parallel electron currents [17], and (5) thermal flux formulas used in radial transport codes with auxiliary heating give good agreement with the measured profiles both in radius and time.

An interpretative simulation with ETG for Tore Supra is shown in Fig. 1 using the CRONOS integrated transport code [5] with a stair stepped Fast Wave heating profi le of 3MW and 6MW. A NSTX High Harmonic Fast Wave heated discharge with $T_{e0} = 4$ keV shows electron transport that is explained by the ETG model. Finally, we can explain how the weakly reversed magnetic shear profi les produced in optimized NSTX/HHFW discharges and fast current ramp TS discharges partially block the transport of electron guiding centers through the formation of a shearless invariant curve in the corresponding drift wave transport model. Weakly reversed magnetic shear discharges in NSTX have shown global electron transport reduced by half, with an associated increase of impurity ions due to an inward electric fi eld. Explanations based on the general principles of dynamical systems are offered for these enhanced electron confi nement regimes.

Acknowledgments

Work supported under the U.S. Department of Energy contract DE-FG02-04ER-54742, the Association Euratom-CEA, CEA/DSM/DRFC CEA France and the Department of Controlled Fusion Research in Commisaire Energy Agency France.

[1] B. B. Kadomtsev. *Tokamak Plasmas : A Complex Physical System*, pages 124–150. Institute for Physics Publishing, Bristol, 1992.

[2] G. T. Hoang, C. Bourdelle, X. Garbet, G. Giruzzi, T. Aniel, M. Ottaviani, W. Horton, P. Zhu, and R. Budny. *Phys. Rev. Lett.*, 87(12):125001–1, 2001.

[3] G. T. Hoang, W. Horton, C. Bourdelle, B. Hu, X. Garbet, and M. Ottaviani. *Phys. Plasmas*, 10(2):604, 2003.

[4] W. Horton, G.T. Hoang, C. Bourdelle, X. Garbet, M. Ottaviani, and L. Colas. *Phys. Plasmas*, 11:2600, 2004.

[5] V. Basiuk, J.F. Artaud, F. Imbeaux, X. Litaudon, A. Bcoulet, L.G. Eriksson, G.T. Hoang, G. Huysmans, D. Mazon, D. Moreau, and Y. Peysson. *Nucl. Fusion*, 43(9):822–830, 2003.

[6] B.P. LeBlanc and *et al.*. *Nucl. Fusion*, 44:513–523, 2004.

[7] G.G. Hoang, C. Bourdelle, X. Garbet, G. Antar, and *et al.*. *Phys. Rev. Lett.*, 84:4593, 2000.

[8] J. M. Kwon, W. Horton, P. Zhu, P. J. Morrison, H. B. Park, and D. I. Choi. *Phys. Plasmas*, 7:1169, 2000.

[9] D. del Castillo-Negrete and P.J. Morrison. *Phys. Fluids*, 5:4, 1993.

[10] J.M. Greene. *J. Math Phys.*, 20:1183, 1979.

[11] A. Apte, A. Wurm, and P. J. Morrison. *Chaos*, 13:421, 2003.

[12] Ongena J., Evrard M., and McCune D. Numerical transport codes. volume 33, pages 181–191. Transactions of Fusion Technology, 1998.

[13] C. Holland and P.H. Diamond. *Phys. Plasmas*, 11(3):1043, 2004.

[14] X. L. Zou, L. Colas, M. Paume, J. M. Chareau, L. Laurent, P. Devynck, and D. Gresillon. *Phys. Rev. Lett.*, 75:1090, 1995.

[15] P. Devynck, X. L. Zou F. Clairet, and et al. *Plasma Phys. Control. Fusion*, 39:1355, 1997.

[16] L. Colas, X. L. Zou, M. Paume, L. Guiziou J. M. Chareau, G. T. Hoang, Y. Michelet, and D. Grsilion. *Nucl. Fusion*, 38:903, 1998.

[17] K. L. Wong, K. Itoh, S.I. Itoh, A. Fukuyama, and M. Yagi. *Phys. Lett. A*, 276:280–285, 2000.